Biosensors and Bioelectronics 27 (2011) 82–87

Contents lists available at ScienceDirect

Biosensors and Bioelectronics

journal homepage: www.elsevier.com/locate/bios

Controlled immobilization of acetylcholinesterase on improved hydrophobic gold nanoparticle/Prussian blue modified surface for ultra-trace organophosphate pesticide detection

Shuo Wu[a,*], Xiaoqin Lan[a], Wei Zhao[b], Yuping Li[c], Lihui Zhang[a], Hainan Wang[a], Mei Han[a], Shengyang Tao[a]

[a] School of Chemistry, Dalian University of Technology, Linggong Road, Dalian 116023, PR China
[b] Institute of Surface Chemistry and Catalysis, Ulm University, D-89069 Ulm, Germany
[c] School of Materials Science and Engineering, Dalian University of Technology, Dalian 116023, PR China

ARTICLE INFO

Article history:
Received 30 January 2011
Received in revised form 15 June 2011
Accepted 16 June 2011
Available online 23 June 2011

Keywords:
Acetylcholinesterase
Orientated immobilization
Improved hydrophobic interface
Organophosphate pesticide
Ultra-low limit of detection

ABSTRACT

An ultrasensitive amperometric acetylcholinesterase (AChE) biosensor was fabricated by controlled immobilization of AChE on gold nanoparticles/poly(dimethyldiallylammonium chloride) protected Prussian blue (Au–PDDA–PB) nanocomposite modified electrode surface for the detection of organophorous pesticide. The Au–PDDA–PB membrane served as an excellent matrix for the immobilization of enzyme, which not only enhanced electron transfer but also possessed a relatively large surface area. In addition, the surface hydrophilicity of the Au–PDDA–PB nanocomposite was finely controlled in the static water contact angle range of 25.6–78.1° by adjusting the ratio of gold nanoparticles to PDDA–PB. On an optimized hydrophobic surface, the AChE adopts an orientation with both good activity and stability, which has been proven by electrochemical methods. Benefit from the advantages of the Au–PDDA–PB nanocomposite and the good activity and stability of AChE, the biosensor shows significantly improved sensitivity to monocrotophos, a typical highly toxic organophorous pesticide, with wide linear range (1.0–1000 pg/mL and 1.0–10 ng/mL) and an ultra-low detection limit of 0.8 pg/mL. The biosensor exhibits accuracy, good reproducibility and stability. This strategy may therefore provide useful information for the controlled immobilization of protein and the design of highly sensitive biosensors.

1. Introduction

Ultra-sensitive detection of neurotoxic organophosphorous compounds (OPs) attracted great attention in the past couple of decades not only because neurotoxins are widely used in the agricultural industry and as chemical warfare agents (Du et al., 2009; Upadhyay et al., 2009; Wang et al., 2008a), but also some of them have very long lifetimes and may find their way in our food and water supplies (Du et al., 2009; Smalling et al., 2010). Recent studies revealed that infant and children were more susceptible to the long-term action of OPs in low concentrations (Larsen and Pascal, 1998). In short, for environmental protection and human health safety purposes, it is necessary to restrict the recommend level of OPs and at the same time develop sensitive and fast technology to monitor OPs infield. Traditional analyzers such as liquid (Ye et al., 2009) or gas chromatography (Guan et al., 2010) coupled with mass spectrometry could detect OPs in ppb levels in dedicated centralized laboratories but encumbered by their complicated sample treatment process and limited sensitivity. Rapid or field biomonitoring tool with ultrahigh sensitivity for the fast responders is always highly desirable.

Recently, electrochemical biosensors with the merits of simple operation procedure, reagentless detection, and low cost, have been well established as promising analysis devices for the analyses of a wide range of biomedical and industrial samples. Among them, the enzyme based electrochemical biosensors are particularly attractive because of the high sensitivity and fast response (Davis et al., 2007; Du et al., 2010; Liu and Lin, 2006; Sun and Wang, 2010; Viswanathan et al., 2009). For the ultra-sensitive detection of OPs, acetylcholinesterase (AChE), a commercial available enzyme, was usually used based on the inhibition of the AChE by these compounds. The properties such as sensitivity and stability of enzyme-based biosensor depend on the immobilization of enzyme, which requires adequate amount and well maintained biological activity. To maintain the nature of enzyme, it is necessary to choose adequate supporting materials and immobilization procedure (Du et al., 2007; Kandimalla and Ju, 2006; Sotiropoulou and Chaniotakis, 2005; Shan et al., 2007; Zhao et al., 2009). Recently,

* Corresponding author. Tel.: +86 411 84986044; fax: +86 411 84838521.
E-mail address: wushuo@dlut.edu.cn (S. Wu).

0956-5663/$ – see front matter © 2011 Elsevier B.V. All rights reserved.
doi:10.1016/j.bios.2011.06.020

studies revealed that hydrophilic surface was better for enzyme immobilization, which was considered as a biocompatible surface to maintain the activity of enzyme (Du et al., 2007; Wu et al., 2007). In some case, the oriented immobilization of enzyme on the hydrophobic surface brought dramatically improved enzyme activity (Palomo et al., 2002). It is also demonstrated that hydrophobic interaction could contribute to the enzyme adsorption (Lee et al., 2003). Therefore, it would be scientifically interesting to adjust the hydrophilicity/hydrophobicity of the electrode surface for the controlled adsorption of AChE to improve the sensitivity of the biosensor. The evaluation of hydrophilicity is based on water contact angle (CA) measurements. In general, the limit between the hydrophilic/hydrophobic interfaces is 90°. In recent years, some researches demonstrated that the limit of hydrophilicity and hydrophobicity should be 65° (Vogler, 1998). According to the new limit, the hydrophobic range is broadened.

Besides the suitable interfacial property, to enhance the sensitivity of the electrode-based biosensors, it is necessary to utilize advanced materials to improve the electron transfer rate between the enzyme and the electrode surface. In this aspect, gold nanoparticles and Prussian blue nanoparticles, which have been successfully used for the fabrication of highly sensitive AChE based electrochemical biosensors (Luckham and Brennan, 2010; Yin et al., 2009; Sun and Wang, 2010), attracted high interest because of their good conductivities and electrocatalytic abilities.

Herein, the wettability of gold nanoparticles/poly(dimethyldiallylammonium chloride) protected Prussian blue (Au–PDDA–PB) modified surface was finely tailored in the static contact angle range of 25.6–78.1° by changing the ratio of the negatively charged gold nanoparticle and the positively charged PDDA–PB. The selection of gold and PB nanoparticle was because of their good conductivity and widely successful application as enzyme immobilized matrix. The influence of the surface hydrophilicity on AChE immobilization and their further electrochemical performance was investigated. An improved hydrophobic surface was more suitable for enzyme immobilization. Under optimal conditions, the AChE biosensor showed ultrahigh sensitivity and good stability. The limit of detection of this biosensor has been lowered down to 0.8 pg/mL, which is much lower than most of the AChE based biosensor. Therefore, this strategy may provide useful information for the controlled immobilization of protein and the design of highly sensitive biosensors.

2. Experimental

2.1. Materials and reagents

AChE (236 U/mg) and acetylthiocholine chloride (ATCl) were purchased from Sigma–Aldrich (St. Louis, USA) and used as received. Monocrotophos was provided by Treechem Co. (Shanghai, China). Poly (vinyl alcohol) (PVA) and PDDA was purchased from BASF (Germany). All other reagents were of analytical grade and used without further purification. 0.1 M phosphate buffer saline (PBS) was prepared by mixing the stock solutions of NaH_2PO_4 and Na_2HPO_4. Doubly distilled water was used in all experiments. The monocrotophos solutions were prepared by a step-dilution method. In detail, 1.0 mL of the standard monocrotophos solution (100 ppm) was totally transferred into a 100.0 mL volumetric flask and diluted for 100 times. Then, 1.0 mL of the obtained solution (1.0 ppm) was further diluted for 100 times. After that, the 10 ng/mL solution was followed with 4-series of 10-fold dilutions to obtain the solutions with concentrations of 1000, 100, 10, and 1.0 pg/mL. To reduce the errors, the glassware used in the experiments, which involving pipettes (2.0 mL and 1.0 mL) and volumetric flasks (100 mL and 5 mL) were all corrected. And the specific concentrations in the low concentration range were verified by UV–vis spectra, as shown in Table S1.

2.2. Apparatus

The static water contact angles were measured with a commercial instrument (CAM 200, KSV Instruments Ltd., Helsinki, Finland). The electrochemical measurements were carried out on a CHI 660C electrochemical working station (CH Instruments Co., Shanghai Chenhua). TEM images were measured at a transition electron microscopy (Tecnai G220 S-Twin, FEI, USA). UV–vis spectrometry (UV-1201, Ruili, Beijing) was utilized for low concentration validation. A three-electrode system was employed with AChE–Au–PDDA–PB/GCE as working electrode, a saturated calomel electrode (SCE) as reference electrode and a platinum wire as counter electrode.

2.3. Inhibition measurement using AChE based biosensor

The performance of the biosensor was tested by its differential pulse voltammetry (DPV) response in pH 8.5 PBS solution containing 1.2 mM ATCl at 700 mV (versus SCE). For inhibition tests, the original DPV signal ($I_{P,control}$) was first measured at 1.2 mM ATCl. Then the electrode was rinsed with water and incubated in an aqueous solution containing the desired concentration of monocrotophos for 10 min. After incubation, the residual signal ($I_{P,exp}$) was recorded at the same condition as the original one. The inhibition rate of monocrotophos was calculated as follows:

$$\text{Inhibition}\,(\%) = \frac{I_{P,control} - I_{P,exp}}{I_{P,control}} 100\%$$

2.4. Synthesis of PDDA–PB nanocomposite.

PDDA–PB nanoparticles were synthesized by a reported method (Uemura et al., 2004). In detail, 4.0 mL of 0.025 M $K_3Fe(CN)_6$ was slowly added to 16 mL of 6.25 M $FeCl_2{\cdot}4H_2O$ containing 0.4% PDDA under vigorous stirring at room temperature. The resulting dark blue colloidal solution was used as a PDDA–PB stock solution. Then Acetone was added into the resulting PB solutions to precipitate the PDDA–PB and remove the residual KCl. After being cleaned with acetone for several times, the PDDA–PB nanocomposite were left and dried in room temperature, then redispersed in water.

2.5. Synthesis of 4 nm gold nanoparticles (AuNPs)

The negatively charged 4 nm AuNPs were synthesized by the method of Gole and Murphy (2004). Typically, 20 mL aqueous solution containing 0.25 mM $HAuCl_4$ and trisodium citrate were mixed and stirred at 4 °C, then 0.6 mL of ice cold 0.1 M $NaBH_4$ was added into this solution with strong stirring. The solution immediately turned orange–red, indicating the formation of gold nanoparticles.

2.6. Synthesis of Au_x–PDDA–PB nanocomposite and fabrication of the AChE–Au_x–PDDA–PB modified electrode

Au_x–PDDA–PB nanocomposites were prepared by simply ultrasonicating the AuNPs and PB–PDDA mixture with aliquot ratios for 30 min, where x represents the volume ratio of AuNPs to PDDA–PB. For the preparation of biosensors, 3 μL of the AChE loaded Au_x–PDDA–PB solution containing 0.5% PVA aqueous solution was subsequently cast on a carefully polished glassy carbon electrodes (GCE, 3 mm in diameter) to obtain the AChE–Au_x–PDDA–PB/GCE. The PVA membrane could fix the AChE immobilized Au_x–PB–PDDA

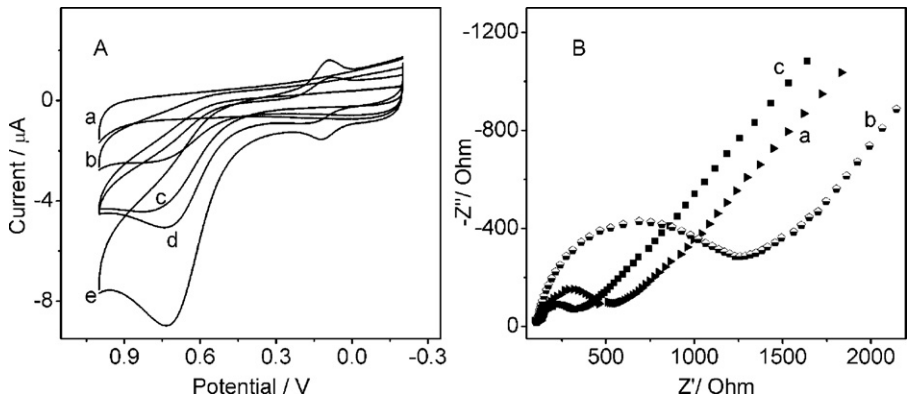

Fig. 1. (A) CVs of AChE–PVA/GCE in the absence (a) and presence (b) of 1.2 mM ATCl, and AChE–AuNP/GCE (c), AChE–PDDA–PB/GCE (d), and AChE–Au_6–PDDA–PB/GCE in the presence of 1.2 mM ATCl in pH 8.5 PBS at 100 mV/s, and (B) Electrochemical impedance spectra of bare GCE (a), PDDA–PB/GCE (b), and Au_6–PDDA–PB/GCE (c) in 5 mM $Fe(CN)_6^{3-/4-}$.

nanocomposite on electrode surface. The biosensor was stored at 4 °C when not in use. For comparison, Au_x–PDDA–PB/GCE, AChE–AuNPs/GCE, and AChE–PDDA–PB/GCE were fabricated.

3. Results and discussion

3.1. Characterization of the gold nanoparticle, PDDA–PB, and Au_6–PDDA–PB

Fig. S1A–C shows the TEM images of the as-prepared gold nanoparticles, PDDA–PB nanomaterials, and the Au_6–PDDA–PB nanocomposite, respectively. The as-prepared gold nanoparticles with a particle size of 4–7 nm were observed, without obvious aggregation. The PDDA–PB nanomaterials were belt shaped, and about 20–30 nm in width. After the negatively charged gold nanoparticles were added into the positively charged PDDA–PB matrix, small black dots were observed in the PDDA–PB matrix, indicating the formation of the Au_6–PDDA–PB nanocomposite.

3.2. Electrochemical characterization of the bio-nanocomposite interface

Fig. 1A shows the cyclic voltammograms (CVs) of AChE–PVA/GCE in the presence and absence of 1.2 mM ATCl, and AChE–PDDA–PB/GCE, AChE–AuNP/GCE and AChE–Au_6–PDDA–PB/GCE in the presence of 1.2 mM ATCl in pH 8.5 PBS at 100 mV/s. Without addition of ATCl, no peak was observed at AChE–PVA/GCE in PBS. When 1.2 mM ATCl was added into the PBS, an increased irreversible oxidation peak at 680 mV emerged, which was ascribed to the oxidation of thiocholine, hydrolysis product of ATCl, catalyzed by immobilized AChE. Compared with AChE–PVA/GCE, the peak currents increased sharply on the electrode with PDDA–PB or AuNPs. It is estimated that the addition of PDDA–PB and gold nanoparticles possessed a relatively large specific surface area, which greatly enhance the immobilized amount of AChE. The other reason would be the electron transfer rate of the composite membrane should be enhanced with the addition of nanoparticles with good electronic conductivity, which will be discussed further. It should be noticed that there is a significant increase of peak current on AChE–Au_6–PDDA–PB/GCE, which is attributed to the combination of AuNPs and PB–PDDA, which leads to synergistic effect of the nanoparticles. The pair of redox peaks centered at 185 and 202 mV on AChE–PDDA–PB/GCE and AChE–Au_6–PDDA–PB/GCE are attributed to the reduction and oxidation of PB (Zhao et al., 2005).

The electron transfer rate of the nanocomposite interface was examined by electrochemical impedance spectra (EIS). Fig. 1B shows the electrochemical impedance spectra (EIS) of bare GCE, PDDA–PB/GCE, and Au_6–PDDA–PB/GCE using $Fe(CN)_6^{3-/4-}$ redox couple as an indicator. The Nyquist plot of the EIS includes a semicircular portion and a linear portion. The semicircular portion at higher frequencies corresponds to the electron-transfer-limited process and its diameter is equal to the electron transfer resistance (*R*ct), which controls the electron-transfer kinetics of the redox probe at the electrode interface (Bard and Faulkner, 2001). The electron-transfer resistance of the bare GCE, PDDA–PB/GCE, and Au_6–PDDA–PB/GCE were 150, 1200, and 350 Ω, respectively. It is clear that the electron transfer would be slower down by the modification of additional membrane on the surface of GCE, but the introduction of AuNPs in the nanocomposite will definitely improve the electron transfer rate of the membrane.

3.3. Alteration of surface hydrophilicity and its application in AChE immobilization

Fig. 2A shows the static water contact angles (CAs) of the AuNPs, PDDA–PB, and Au_6–PDDA–PB modified glassy carbon sheet surface. The CAs of AuNPs and PDDA–PB modified glassy sheet surface were 29.2° and 32.7°, respectively, indicating the good hydrophilicity. When adding optimized aliquot amount of AuNPs in PDDA–PB, the CA of Au_6–PDDA–PB modified surface significantly increased to 78.1°, indicating the formation of an improved hydrophobic surface. There was no direct proof for the explanation of this phenomenon. We assumed it was attributed to the orientation change of the PDDA groups, including hydrophilic $(CH_3)_4N^+$ and hydrophobic carbon chain (see Fig. 2B). As shown in Fig. 2B, before AuNPs assembly, the surface was hydrophilic, which could be induced by the domination of $(CH_3)_4N^+$ on the surface that forming hydrogen bonds with water. In addition, the positively charged group would repulse each other thus also lead to a high surface free energy and small water CA. After the electrostatic assembly of the mixture of negatively charged AuNPs and positively charged PDDA, the nitrogen five-membered ring combined with the surface of AuNPs and embedded in the film. Therefore, the surface of membrane might be dominated by the ($\mathrm{—CH_2CHCHCH_2—}$) which was hydrophobic, thus lead to a low surface free energy and larger CA.

The surface hydrophilic property was influenced by the ratio of AuNPs to PDDA–PB, as shown in Fig. 2C. With increase of the amount of AuNPs, the CAs initially increased from 25.6° to 78.1°, and reached the maximum value of 78.1°at the AuNPs: PDDA–PB ratio of 6 (v/v). Further increase of AuNPs on PDDA–PB surface

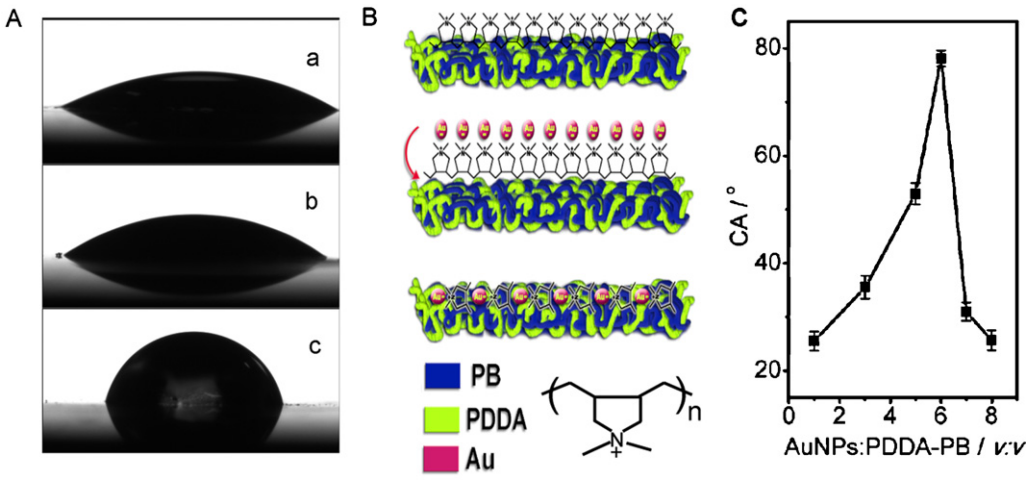

Fig. 2. (A) Contact angles of AuNPs (a), PDDA–PB (b), and Au_6–PDDA–PB (c) films. (B) Scheme of the PDDA–PB interface before and after AuNPs assembly. (C) Influences of AuNPs to PDDA–PB ratio on the static water contact angle.

led to the decrease of the CA. This phenomenon may because at the initial stage, AuNPs induced partial PDDA groups to change their orientations. With the increase of AuNPs, the conformation of PDDA changed more and more and resulted in increasing CA. Over the ratio of 6, further addition of AuNPs would lead to the excess of AuNPs and the surface property might be dominated by the hydrophilic AuNPs, thus resulted in the decrease of the CA. In summary, by tailoring the ratio of AuNPs and PDDA–PB, the CAs could be finely controlled in a range almost covering the domain from hydrophilic to near hydrophobic and would be very useful for the control of enzyme immobilization.

The activity of the AChE based on different modified electrodes with different ratios of AuNPs to PDDA–PB were monitored by comparing the detecting sensitivities to ATCl at 0.7 V in pH 8.5 PBS solution, as shown in Fig. 3A. The trend of the sensitivities according to the increase of AuNPs amount was quite close to that of CAs. The highest sensitivity was obtained at the electrode modified with Au_6–PDDA–PB, which was obtained with biosensor with the most hydrophobic surface. This phenomenon indicated that the improved hydrophobicity of the surface would enhance the immobilized amount and activity of AChE by strong hydrophobic/hydrophobic interaction between the enzyme and the nanocomposite membrane.

According to the reports on the microstructure of AChE by Sussman et al. (1991), the hydrophobic groups of AChE are mostly distributed around its active center, which is a 2 nm deep active site gorge. The hydrophobicity of AChE around the active center is obviously stronger than that on the other part of enzyme, such as its inverse side. Therefore, the orientation of AChE on the solid substrates with different hydrophilicity could be different and thus influence its activity and stability. Here, the optimal detecting pH values based on biosensors with different surface hydrophilicity were kind of different and altered from 8.0 to 8.5 (see Fig. 3B), which indicated the different activity and stability of AChE on the surface of electrodes. The highest pH value was achieved at the most hydrophobic surface. The optimal pH value of the AChE modified electrode depended on two factors. On one hand, the electrochemical oxidation of thiocholine could be promoted by increasing the OH^- concentration in the reactive media due to their consumption of the electrochemical generated of H^+ during the electrochemical oxidation process (Wang et al., 2008b). On the other hand, high OH^- concentration has adverse effect on the enzyme activity. Therefore, in this case, the highest pH value achieved at the most hydrophobic surface indicates that the hydrophobic surface was best for stabilizing the enzyme. We assume that on hydrophobic surface, the molecule of AChE may prefer the orientation with

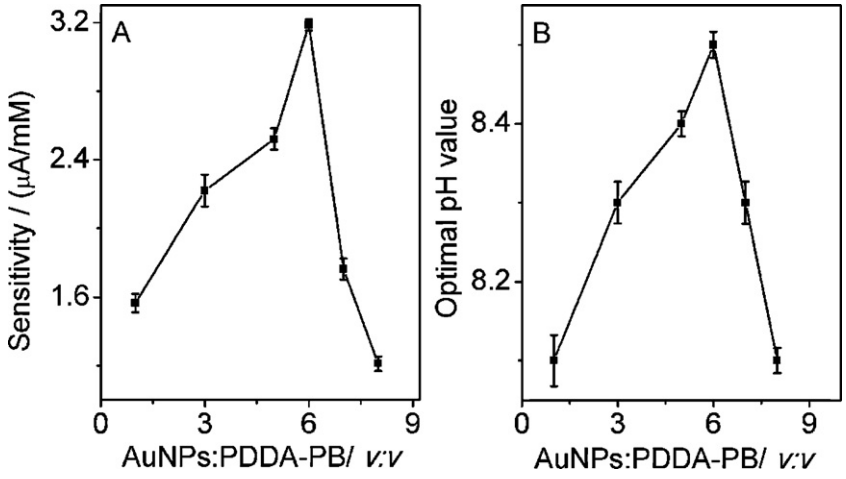

Fig. 3. Influence of AuNPs to PDDA–PB ratio on (A) the sensitivities to ATCl at 0.7 V in pH 8.5 PBS solutions, and (B) the optimal pH values of the AChE biosensors based on different interfaces.

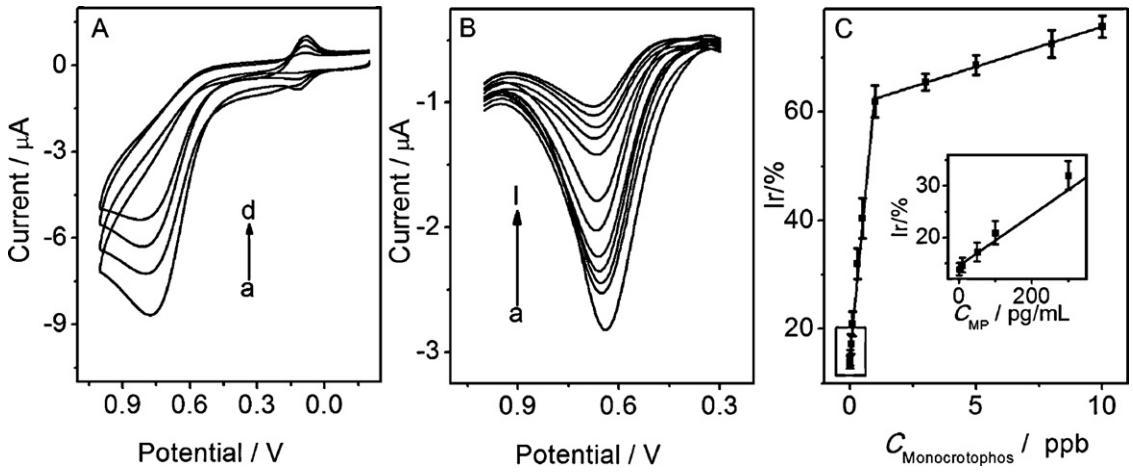

Fig. 4. (A) CVs of AChE–Au_6–PDDA–PB/GCE before and after the inhibition in 10, 100, and 500 pg/mL monocrotophos for 10 min in 0.1 M pH 8.5 PBS containing 1.2 mM ATCl at 100 mV/s. (B) DPV plots of AChE–Au_6–PDDA–PB/GCE before and after inhibition in 1.0, 10, 50, 100, 300, 500, 1000, 3000, 5000, 8000, and 10,000 pg/mL monocrotophos for 10 min (from a to l). (C) Inhibition curve of the AChE–Au_6–PDDA–PB/GCE to monocrotophos with different concentrations. Inset, the amplification of the linear curve in low concentration range.

its active center facing downward to the surface, which makes its active center partially protected thus results in improved stability.

Therefore, evidenced by the sensitivities and stabilities of the biosensors, it is quite reasonable to conclude that the alteration of the surface hydrophilicity would influence the immobilization and orientation of AChE, which correspondingly had direct impact on the performance of the biosensor.

3.4. Detection of ATCl via AChE–Au_6–PDDA–PB/GCE

The sensitivity of the electrochemical biosensor strongly depends on the preparation procedure and detection conditions. To achieve the best response, parameters including the concentration of Au_6–PDDA–PB and the pH value of detecting buffer were optimized. As shown in Fig. S2A and B, the largest amperometric response current of the AChE–Au_6–PDDA–PB/GCE to 1.2 mM ATCl was obtained when the GCE was modified with 3.0 μL 0.8 mg/mL Au_6–PDDA–PB (Au:PDDA–PB = 6:1), and detected in pH 8.5 PBS.

Fig. S3 shows the amperometric response of the AChE biosensor fabricated on the Au_6–PDDA–PB modified electrode. A stepped growth of oxidation current was observed with stepped increase of ATCl concentration in a stirred buffer at 0.7 V. The response was linear in the range of 10 μM–1.0 mM, and got a plateau at 1.2 mM, indicating a typical Michaelis–Menten process. The apparent Michaelis–Menten constant (K_m^{app}) was estimated to be 0.30 mM according to the Lineweaver–Burk equation. The value was lower than those of 0.45 mM for AChE adsorbed on AuNPs–SiSG composite film (Du et al., 2007), and 0.38 mM for AChE adsorbed on mesoporous silica modified electrode (Wu et al., 2011), indicating a high affinity to the substrates. For the further pesticide analysis, 1.2 mM ATCl was then chosen as the uniform concentration in the following experiments.

3.5. Biosensing of monocrotophos on the AChE–Au_6–PDDA–PB/GCE

Monocrotophos is a typical organophosphate pesticide with high toxicity, which could irreversibly inhibit the activity of AChE and form very stable phosphorylated compound with AChE. The good stability of phosphorylated AChE is an advantage for the accurate detection of the specific activity of the enzyme. The inhibition time was a key parameter influencing the inhibition rate of the biosensor. As shown in Fig. S4, with the increase in incubation time the inhibition rate increased and reached a stable value after inhibition of 10 min, thus, 10 min was used for the assay. Fig. 4A shows the response of the biosensor before and after 10 min incubation in 10, 100, and 500 pg/mL monocrotophos solution, the anodic peak currents (curves b–d) dramatically decreased compared with that on the control (curve a), and the decrease in peak current increased with the increasing concentration of monocrotophos. Based on the change in voltammetric signal, the monocrotophos concentration could be precisely detected. Under optimal conditions, the inhibition was proportional to the monocrotophos concentration ranging from 1.0 pg/mL to 1.0 ng/mL ($y = 0.049x + 14.5$, $R^2 = 0.991$, $n = 7$) and from 1.0 ng/mL to 10 ng/mL ($y = 0.0015x + 60.9$, $R^2 = 0.996$, $n = 5$), with the limit of detection of 0.8 pg/mL calculated based on the 3 times of R.S.D., as shown in Fig. 4B and C. The performance of this AChE–Au–PDDA–PB/GCE compared with other reported AChE biosensors is summarized in Table 1. It shows that the present AChE–Au_6–PDDA–PB/GCE exhibited much lower limit of detection,

Table 1
The key parameters of AChE biosensors for pesticide detection.

Methods	Pesticide	Linear range	Detection limit	references
AChE/nano$CaCO_3$–chitosan	Methyl parathion	0.005–0.2; 0.75–3.75 mg/mL	1 ppb	Gong et al. (2009a,b)
AChE/CNT–PDDA layer	Paraoxon	0.3 pg/mL–2.75 ng/mL	0.1 pg/mL	Liu and Lin (2006)
PATP membranes/AuNPs	Chlorpyrifos	0.18–3.5 μg/mL	0.1 μg/mL	Xie et al. (2010)
AChE/chitosan–PB	Dichlorvos, omethoate, trichlorfon, phoxim	0.01–10 ng/mL, 0.05–10 ng/mL, 0.03–5 ng/mL, 0.05–10 ng/mL	2.5 ng/mL, 15 ng/mL, 5.0 ng/mL, 5.0 ng/mL	Sun and Wang (2010)
AChE–AuNPs–Polypyrrole nanowires	Methyl parathion	0.005–0.12 μg/mL, 0.5–4.5 μg/mL	2 ng/mL	Gong et al. (2009a,b)
AChE–Au_6–PDDA–PB	Monocrotophos	1.0–1000 pg/mL, 1.0–10 ng/mL	0.8 pg/mL	Our method

Table 2
Recovery studies of monocrotophos in garlic samples. (Each result was estimated by 6 determinations).

Sample	Taken (pg/mL)	Found (pg/mL)	Recovery (%)	RSD (%)
1	5.00	4.64	92.8	3.2
2	25.0	24.5	98.0	5.8
3	50.0	53.2	106	4.6
4	150	142	94.6	3.9
5	250	265	105	5.3
6	500	515	103	4.7

indicating that this strategy is more suitable of enzyme immobilization and enzyme activity maintenance, which could contribute a lot to the sensitivity enhancement of the biosensor.

3.6. Reproducibility measurements and real sample analysis

The inter-assay precision was estimated at 5 different electrodes for the determinations in 1.2 mM ATCl after being incubated in 1.0 ng/mL monocrotophos solutions for 10 min (Fig. S5). The R.S.D. of inter-assay was found to be 4.8%, as shown in Table S2, indicating the acceptable precision and reproducibility. When the enzyme electrode was not in use, it was stored at 4 °C in dry condition. No obvious decrease in the response of ATCl was observed in the first 7-day storage. After a 30-day storage period, the sensor retained 93.6% of its initial current response.

To further demonstrate the practicality of the proposed biosensor, the recovery test was studied by adding different amounts of monocrotophos into garlic samples. Results are summarized in Table 2. The recoveries were from 92.8% to 106%. The results indicated that the proposed method was highly accurate, precise and reproducible. It could be used for direct analysis of relevant samples.

4. Conclusion

A novel method for finely tailoring the surface hydrophilicity for orientated AChE immobilization and highly sensitive OP detection was developed. By adjusting the ratios of AuNPs to PDDA–PB, the static water contact angle of the Au–PDDA–PB modified surface could be tailored from 25.6° to 78.1° due to the conformation change of the PDDA groups combined with gold nanoparticles. Consequently, AChE preferred to adopt different orientations and adsorbed behaviors on the surfaces with different hydrophilicity/hydrophobicity due to their uneven distribution of hydrophobic groups. Evidenced by the detecting sensitivity and optimal pH value measurements, surface with improved hydrophobic property was more suitable for AChE adsorption, which could both maintain the activity and stability of AChE. Therefore, the optimized AChE–Au_6–PDDA–PB/GCE showed not only ultrahigh sensitivity for the detection of monocrotophos, but also good stability and accuracy. This method would provide a new strategy for the orientated adsorption of proteins, thus would open a new horizon for the construction of ultra-sensitive biosensors.

Acknowledgements

The authors gratefully acknowledge the financial support of the National Natural Science Foundation of China (Nos. 20805003 and 20903018), the Research Fund for the Doctoral Program of Higher Education of China (No. 200801411106), and the Fundamental Research Funds for the Central Universities (893383).

Appendix A. Supplementary data

Supplementary data associated with this article can be found, in the online version, at doi:10.1016/j.bios.2011.06.020.

References

Bard, A.J., Faulkner, L.R., 2001. Electrochemical Methods Fundamentals and Applications. Wiley, NY.
Davis, F., Law, K.A., Chaniotakis, N.A., Fournier, D., Gibson, T., Millner, P., Marty, J.L., Sheehan, M.A., Ogurtsov, V.I., Johnson, G., Griffiths, J., Turner, A.P.F., Higson, S.P. J., 2007. Comprehensive Analytical Chemistry, vol. 49 (Chapter 15), pp. 311–330.
Du, D., Chen, S.Z., Cai, J., Zhang, A.D., 2007. Biosens. Bioelectron. 23, 130–134.
Du, D., Wang, J., Smith, J.N., Timchalk, C., Lin, Y.H., 2009. Anal. Chem. 81, 9314–9320.
Du, D., Ye, X.X., Cai, J., Liu, J., Zhang, A.D., 2010. Biosens. Bioelectron. 25, 2503–2508.
Gong, J.M., Liu, T., Song, D.D., Zhang, X.B., Zhang, L.Z., 2009a. Electrochem. Commun. 11, 1873–1876.
Gong, J.M., Wang, L.Y., Zhang, L.Z., 2009b. Biosens. Bioelectron. 24, 2285–2288.
Gole, A., Murphy, C.J., 2004. Chem. Mater. 16, 3633–3640.
Guan, H.X., Brewer, W.E., Garris, S.T., Morgan, S.L., 2010. J. Chromatogr. A 1217, 1867–1874.
Kandimalla, V.B., Ju, H.X., 2006. Chem.-A Eur. J. 12, 1074–1080.
Larsen, J.C., Pascal, G., 1998. Food Addit. Contam. 15, 1–9.
Lee, Y., Lee, E.K., Cho, Y.W., Matsui, T., Kang, I.C., Kim, T.S., Han, M.H., 2003. Proteomics 3, 2289–2304.
Liu, G.D., Lin, Y.H., 2006. Anal. Chem. 78, 835–843.
Luckham, R.E., Brennan, J.D., 2010. Analyst 135, 2028–2035.
Palomo, J.M., Muñoz, G., Fernández-Lorente, G., Mateo, C., Fernández-Lafuente, R., Guisánl, J.M., 2002. J. Mol. Catal. B: Enzym. 19–20, 279–286.
Shan, D., Han, E., Xue, H.G., Cosnier, S., 2007. Biomacromolecules 8, 3041–3046.
Smalling, K.L., Morgan, S., Kuivila, K.K., 2010. Environ. Toxicol. Chem. 29, 2593–2599.
Sotiropoulou, S., Chaniotakis, N.A., 2005. Anal. Chim. Acta 530, 199–204.
Sussman, J.L., Harel, M., Frolow, F., Oefner, C., Goldman, A., Toker, L., Silman, I., 1991. Science 253, 872–876.
Sun, X., Wang, X.Y., 2010. Biosens. Bioelectron. 25, 2611–2614.
Uemura, T., Ohba, M., Kitagawa, S., 2004. Inorg. Chem. 43, 7339–7345.
Upadhyay, S., Rao, G.R., Sharma, M.K., Bhattacharya, B.K., Rao, V.K., Vijayaraghavan, R., 2009. Biosens. Bioelectron. 25, 832–838.
Viswanathan, S., Radecka, H., Radecki, J., 2009. Biosens. Bioelectron. 24, 2772–2777.
Vogler, E.A., 1998. Adv. Colloid Interface Sci. 74, 69–117.
Xie, C.G., Li, H.F., Li, S.Q., Wu, J., Zhang, Z.P., 2010. Anal. Chem. 82, 241–249.
Ye, J., Wu, J., Liu, W.P., 2009. Trends Anal. Chem. 28, 1148–1163.
Yin, H.S., Ai, S.Y., Xu, J., Shi, W.J., Zhu, L.S., 2009. J. Electroanal. Chem. 637, 21–27.
Wang, H., Wang, J., Timchalk, C., Lin, Y.H., 2008a. Anal. Chem. 80, 8477–8484.
Wang, J., Timchalk, C., Lin, Y.H., 2008b. Environ. Sci. Technol. 42, 2688–2693.
Wu, S., Ju, H.X., Liu, Y., 2007. Adv. Funct. Mater. 17, 585–592.
Wu, S., Zhang, L.L., Qi, L., Tao, S.Y., Lan, X.Q., Liu, Z.G., Meng, C.G., 2011. Biosens. Bioelectron. 26, 2864–2869.
Zhao, W., Ge, P.Y., Xu, J.J., Chen, H.Y., 2009. Environ. Sci. Technol. 43, 6724–6729.
Zhao, W., Xu, J.J., Shi, C.G., Chen, H.Y., 2005. Langmuir 21, 9630–9634.